Наносистеми, наноматеріали, нанотехнології
Nanosistemi, Nanomateriali, Nanotehnologii
2023, т. 21, № 2, сс. 427–449

PACS numbers: 68.37.Lp, 75.50.Tt, 75.60.-d, 75.75.Cd, 81.70.Pg, 82.30.Lp, 82.65.+r

Magnetosensitive Nanocomposite $Fe_3O_4/Al_2O_3/C$ Synthesis and Properties

A. P. Kusyak, N. V. Kusyak, O. I. Oranska, T. V. Kulyk, L. S. Dzubenko, B. B. Palianytsia, O. A. Dudarko, N. M. Korniichuk, A. L. Petranovska, and P. P. Gorbyk

O. O. Chuiko Institute of Surface Chemistry, N.A.S. of Ukraine, 17, General Naumov Str., UA-03164 Kyiv, Ukraine

The processes of carbonization of sucrose-containing coatings on the surface of single-domain magnetite and magnetosensitive nanocomposite (MNC) Fe_3O_4/Al_2O_3 are studied. The MNC with a carbon surface is synthesized by the method of low-temperature pyrolysis of carbohydrates. As revealed, the used heat-treatment mode does not lead to deterioration of the magnetic characteristics of magnetite under the condition of preliminary creation of a protective layer of alumina on its surface. Differential thermal analysis (DTA) in combination with differential thermogravimetric analysis (DTGA) and programmed temperature-desorption mass spectrometry show that the carbonization of sucrose under these conditions is complete. The shape and dimensions of the Fe_3O_4, Fe_3O_4/Al_2O_3 and $Fe_3O_4/Al_2O_3/C$ MNCs are investigated by the TEM method. As established, the values of the specific saturation magnetization of MNCs are consistent with the corresponding changes in the mass fraction of magnetite in the Fe_3O_4/Al_2O_3 and $Fe_3O_4/Al_2O_3/C$ structures. The results of TEM studies and magnetic measurements indicate the formation of the Fe_3O_4/Al_2O_3 and $Fe_3O_4/Al_2O_3/C$ MNCs by the core–shell type. Methylene blue is used to study the adsorption activity of the $Fe_3O_4/Al_2O_3/C$ MNC surface. The results of the work can be used in the development of new magnetically controlled adsorption materials for medical–biological purposes.

Досліджено процеси карбонізації сахарозовмісних покриттів на поверхні однодоменного магнетиту та магнеточутливого нанокомпозиту (МНК) Fe_3O_4/Al_2O_3. Методом низькотемпературної піролізи вуглеводів синтезовано МНК з вуглецевою поверхнею. Встановлено, що використовуваний режим термооброблення не призводить до погіршення магнетних характеристик магнетиту за умови попереднього створення на його поверхні захисного шару оксиду Алюмінію. Диференційна термічна аналіза (ДТА) у поєднанні з диференційною термоґравіметричною

аналізою (ДТҐА) та мас-спектрометрією програмованої температурної десорбції свідчать про повноту карбонізації сахарози за умов експерименту. Методом ПЕМ досліджено форму та розміри МНК Fe_3O_4, Fe_3O_4/Al_2O_3 та $Fe_3O_4/Al_2O_3/C$. Встановлено, що значення питомої намагнетованости наситу МНК узгоджуються з відповідними змінами масової частки магнетиту в структурах Fe_3O_4/Al_2O_3 та $Fe_3O_4/Al_2O_3/C$. Результати ПЕМ-досліджень і магнетних мірянь свідчать про формування МНК Fe_3O_4/Al_2O_3 та $Fe_3O_4/Al_2O_3/C$ за типом ядро–оболонка. Для дослідження адсорбційної активности поверхні МНК $Fe_3O_4/Al_2O_3/C$ використовували метиленовий синій. Результати роботи можуть бути використані для розробки нових магнетокерованих адсорбційних матеріялів медично-біологічного призначення.

Key words: magnetosensitive nanocomposites, carbon surface, pyrolysis, adsorption.

Ключові слова: магнеточутливі нанокомпозити, карбонова поверхня, піроліза, адсорбція.

(Received 20 September, 2022)

1. INTRODUCTION

Analysis of the state of the economy and trends in the modern nanoindustry leads to the conclusion that one of the most promising branches of nanotechnology is the production of carbon nanomaterials for various functional purposes. Carbon is known to form an extremely rich range of structural modifications with unique physical, chemical and biological properties. According to the existing classification, such structures include, in particular: crystalline forms—diamond (cubic structure), graphite (hexagonal structure), carbine (structure of linear chains of carbon atoms packed into crystals by the van der Waals forces); fullerenes (quasi-zero-dimensional structures) and their derivatives—fullerites; carbon fibres and single-walled and multiwalled nanotubes (quasi-one-dimensional structures); graphene (quasi-two-dimensional structures) [1, 2]. Therefore, the growing interest of researchers in the use of various carbon nanostructures in the composition of nanocomposites (NCs) is natural [3–8].

In particular, carbon nanomaterials and NCs based on them, including magnetosensitive ones, are in growing demand in engineering, biotechnology, medicine, environmental protection, *etc.* [1–3, 9–13]. Thus, magnetosensitive NCs with carbon components are used in the development of new types of carriers for targeted delivery of drugs, contrast agents for magnetic resonance imaging, medical hyperthermia, magnetically controlled adsorbents for various

functional purposes. Carbon coatings are able to perform unique functions in the composition of NCs and protect them from the aggressive action of acidic and alkaline environments [14].

Among the nanodisperse magnetically sensitive materials used to create multifunctional MNCs, magnetite (Fe_3O_4) and its modified forms occupy an important place due to their unique physicochemical and biological properties [15–20]. In particular, MNCs based on single-domain Fe_3O_4 with a core–shell structure and hierarchical multilevel nanoarchitecture are capable to performing a theranostic complex of functions characteristic of medical–biological nanorobots [20–30]: recognition of microbiological objects in biological environments; targeted delivery of drugs to target cells and organs and deposition; complex local chemo-, immuno-, neutron-capture-, hyperthermic-, photodynamic therapy and real-time diagnostics; detoxification of the body by adsorption of cell decomposition residues, viral particles, heavy metal ions, *etc.* and their removal by magnetic field.

The result of surface modification is a decrease of the aggregation of magnetite nanoparticles (MNPs) and an increase of the specific surface area of MNCs [31], which allows optimizing the magnetic and adsorption properties [32]. Such MNCs exhibiting a high adsorption capacity can be controlled by a magnetic field, and the stage of separation of the spent adsorbent can be performed by the method of magnetic separation.

The aim of this work is the synthesis of promising for practical use magnetosensitive MNCs with a structure of the core–shell type based on single-domain magnetite and carbon, the study of their adsorption activity and magnetic properties.

2. EXPERIMENTAL SECTION

The most common one-step method for the synthesis of carbon-containing NCs is hydrothermal (solvothermal) [33–35]. The disadvantage of this method is the formation of a mixture of organic compounds on the surface of magnetic particles [36]. The controlled carbonization process due to changes in reaction conditions and environment occurs when mixing pre-synthesized magnetic NPs with a carbon source (*e.g.*, glucose, dopamine and ethylene glycol) [37, 38].

In this work, nanosize single-domain Fe_3O_4 in the superparamagnetic state was used as a magnetically sensitive mineral matrix for the synthesis of core–shell type structures with a carbon surface. Such MNPs became uniformly magnetized throughout the volume at any values and directions of the external magnetic field **H** [25–27, 29].

Obtaining MNCs with a carbon shell is possible by pyrolysis of the carbohydrate layer deposited on its surface. Pyrolysis at temperatures from 400 to 550°C was considered low-temperature, and at temperatures from 600 to 1000°C and higher, as high-temperature one. At higher temperature, the carbonization process was faster. Glucose, sucrose, starch and CS polygel (carbomer 934) were previously investigated as a carbon source [16]. It is was established that using sucrose as a carbon source, due to it physicochemical and thermal properties, carbon yield and properties of the obtained carbon coatings, was advisable. Magnetite, in the absence of oxygen, was characterized by the preservation of ferromagnetic properties to the Curie point (585°C) and by the preservation of the reversibility of magnetothermal characteristics after heating to 800°C. Due to the oxidation of magnetite in the air, phase transitions were recorded as the formation of maghemite (γ-Fe_2O_3) at temperatures of 250–300°C and hematite (α-Fe_2O_3) at temperatures above 350°C [39] that leaded to a significant deterioration of magnetic properties. To stabilize the chemical composition and magnetic properties around the Fe_3O_4 nucleus, oxide shells were created, for example, SiO_2 [16].

Previous research has shown that the best way to achieve this goal may be the use of magnetite with a modified alumina (Al_2O_3) surface. Thus, the Fe_3O_4/Al_2O_3 MNCs were characterized by thermal stability sufficient to preserve the magnetic properties of the NC core by heat treatments in the range of sucrose pyrolysis temperatures during the formation of carbon coatings in the $Fe_3O_4/Al_2O_3/C$ MNCs' structure.

2.1. Synthesis of Nanodispersed Fe_3O_4

Nanodispersed magnetite was synthesized by the Elmore reaction [20]:

$$Fe^{2+} + 2Fe^{3+} + 8NH_4OH \rightarrow Fe_3O_4 + 4H_2O + 8NH_4^+.$$

The NPs Fe_3O_4 ensemble was characterized by sizes of 3–23 nm, and their average size (D_{XRD}) determined by Scherrer's formula was of 10.5 nm. The specific surface area, estimated by the formula $S_{sp} = 6/(\rho D_{XRD})$, where ρ is the particle density, was of 110 $m^2 \cdot g^{-1}$. The values of the coercive force $H_c = 81.0$ Oe, the saturation magnetization $\sigma_s = 55.6$ emu$\cdot g^{-1}$ were characteristic of Fe_3O_4 NPs in the absolutely single-domain state. The presence of OH groups on the surface of magnetite (2.2 mmole/g) was determined using IR spectra. The synthesis and properties of magnetite are described in more detail in Refs. [27, 29].

2.2. Synthesis of Fe_3O_4/Al_2O_3 MNCs

The isopropyl alcohol was added to the highly dispersed magnetite and stirred for 15 min to form a stable suspension. Three times more aluminium isopropylate $(C_3H_7O)_3Al$ was calculated relative to the number of hydroxyl groups of magnetite surface; the overage was added to the suspension.

The weight of the modifier was calculated by the formula

$$m = ngAM, \quad (1)$$

where M is the molecular weight of the modifier; A is the number of hydroxyl groups on the surface of magnetite [mole]; $n = 3$ is excess modifier; g is weight of the carrier (magnetite) [g].

The modification was performed in a boiling mixture with stirring for 6 h. The obtained NCs were separated by decantation on a permanent magnet, washed with isopropyl alcohol until a negative reaction of the washing liquid on Al (III) (0.1% solution of alizarin red) and dried in air for 24 h.

The synthesis of aluminium-containing coating on the surface of Fe_3O_4 was carried out by two time chemical modification with aluminium isopropylate. As a result of the polycondensation reaction, the surface of magnetite acquires an amphoteric character due to Al–(OH)– groups [41]. The polycondensation reaction can be represented by the scheme:

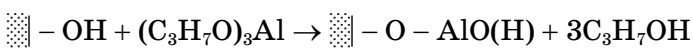

2.3. Synthesis of $Fe_3O_4/Al_2O_3/C$ MNCs

The obtained Fe_3O_4/Al_2O_3 NCs was impregnated using a rotary evaporator with sucrose solutions at the rate of 0.45 g of carbohydrate per 1 g of NCs. Carbonization of the carbohydrate shell of NCs was carried out in argon at 500°C for 2 h in a furnace with programmable heating (heating rate—10 deg·min^{-1}).

2.4. Research Methods

The crystal structure of NPs was determined by x-ray diffraction (XRD). XRD measurements were performed using DRON-4-07 diffractometer with CoK_α radiation and Fe filter focusing on Bragg–Brentano.

Structural studies of NPs and modified ones were performed by powder x-ray diffraction method (XRD) using DRON-UM1 diffrac-

tometer ('Burevestnik', Russia) with Fe-filtered CoK_α radiation focusing on Bragg–Brentano in 2θ range of 10–80°.

The specific surface of the samples was determined by the method of adsorption–desorption of nitrogen using KELVIN 1042 Sorptometer 'COSTECH Instruments' at the boiling point of liquid nitrogen. The sorbents were previously degassed in a helium stream at 110°C.

$$S_{sp} = A_\infty N_A \omega_m, \tag{2}$$

where S_{sp} is the specific surface area of the adsorbent [$m^2 \cdot g^{-1}$]; A_∞ is limiting value of adsorption [$mole \cdot g^{-1}$]; N_A is the Avogadro constant, ($6.022 \cdot 10^{23}$ $mole^{-1}$); ω_m is the area of the adsorbate molecule [$Å^2$].

The specific surface area of the original magnetite was of 110 $m^2 \cdot g^{-1}$, the volume of micropores was of 1.16 mm^3, the surface area of micropores was of 3.30 $m^2 \cdot g^{-1}$.

Determination of the possible presence of organic residues on the surface of the NCs as a result of insufficiently deep destruction of the organic phase of the modifier in the process of pyrolysis of composites was studied by temperature-programmable desorption mass spectrometry (MX-7304A, Sumy, Ukraine) with electron impact ionization [41, 42]. A sample weighing 10–20 mg was placed on the bottom of a quartz–molybdenum ampoule at a pressure of $\cong 5 \cdot 10^{-5}$ Pa. Programmable linear heating of the sample was performed at a rate of 0.17°C·s^{-1} to a temperature of ≅ 750°C. The registration of mass spectra was carried out in the range of 1–210 amu. About 240 mass spectra were recorded during the experiment.

The method of differential thermal analysis (DTA) in combination with differential thermogravimetric analysis (DTGA) was used to study thermal transformations in NCs. The thermograms were recorded using a Q-1500D derivatograph (MOM, Hungary) in the temperature range of 20–1000°C at a heating rate of 10°C·min^{-1}.

Investigations of morphology and size distribution of NPs were performed in water solutions. The size and shape of the NPs were determined by electron-microscopy methods using transmission electron microscope JEOL 1200 EX (Tokyo, Japan) with a tungsten filament operating at a 120 kV acceleration voltage. The TEM samples were diluted in deionizer water, dropping it onto a carbon coated copper grid (EM Resolutions Ltd) and were dried at room temperature for 12 h.

The magnetization of the samples was measured using a vibrating magnetometer at a frequency of 228 Hz at room temperature as described in Ref. [24]. Samples for research were dry demagnetized polydisperse materials. For comparing, Ni sample and Fe_3O_4 (98%)

nanoparticles ('Nanostructured&Amorphous Materials Inc', USA) were used. The measurement error did not exceed 2.5%.

The adsorption capacity was estimated using methylene blue (MB). Optical density measurements and concentration in solutions were performed by spectrophotometric analysis using spectrometer Lambda 35 UV/Vis (Perkin Elmer Instruments). To study the processes of MB adsorption on the surface of MNPs, the series of samples ($g = 30$ mg) with different concentrations in the range of 0.002–0.150 mg·mL^{-1} were made ($V = 5$ mL, pH = 7.0).

MB adsorption was performed for 3 h in static mode at room temperature. The amount of adsorbed MB on the surface of nanocomposites was determined by measuring the concentration of the solutions before and after adsorption. The concentration was determined by spectrophotometric measurements at $\lambda = 590$ nm using the calibration graph method.

The adsorption capacity A [mg·g^{-1}] is calculated using Eq. (3):

$$A = (C_0 - C_{eq})V/m, \tag{3}$$

where A [mg·g^{-1}] is the amount adsorbed; C_0 and C_{eq} [mg·L^{-1}] are the initial and equilibrium concentration of the solution; V [mL] is the volume of the solution; g [g] is the mass of absorbent used.

The removal efficiency of MB, R, was obtained with Eq. (4):

$$R = \{(C_0 - C_{eq})/C_0\}\cdot 100\%. \tag{4}$$

3. RESULTS AND DISCUSSION

The influence of sucrose content, pressure (p), temperature (t) and pyrolysis time (τ) on the structure of magnetite and the composition of the carbon shell during thermal transformations of magnetite and carbohydrates on the surface was studied.

According to XRD analysis, the crystal structure of the original Fe_3O_4 was characterized by clear reflexes, the most intense of which are at $2\theta = 35.5°$, 41.5°, 50.1°. The data found (Fig. 1, *a*) are in good agreement with the crystallographic data of the magnetite phases (JCPDS No. 88-315).

Results of XRD studies for samples with carbon shell obtained by pyrolysis of magnetite/sucrose NCs (magnetite:carbohydrate mass ratio is 1.00/0.45, $t = 200$°C, $p = 506.6$ kPa, $\tau = 6$ h, environment argon) is shown in Fig. 1, *b*.

XRD study of samples of NCs obtained under these pyrolysis conditions indicates the preservation of the magnetite phase and the formation of the γ-Fe_2O_3 phase ((JCPDS No. 39-1346) (Fig. 1, *b*).

Organic residues in the composition of the carbon shell formed on

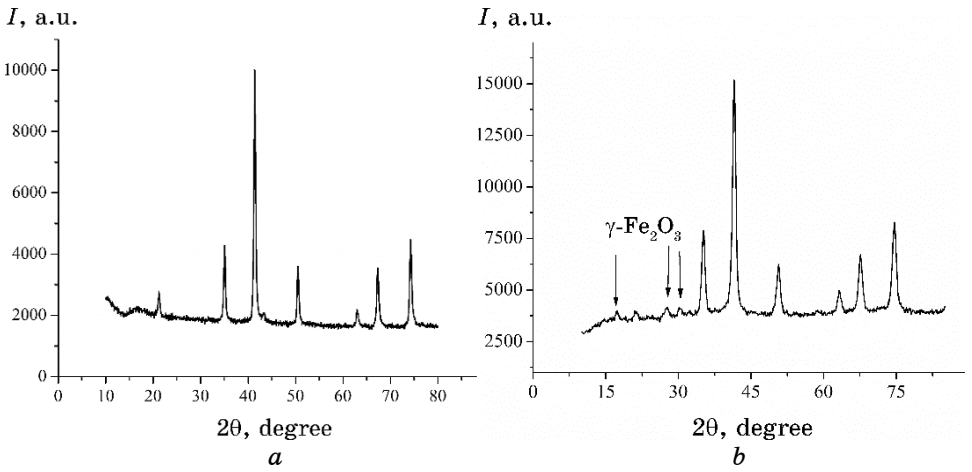

Fig. 1. XRD patterns of MNPs: of the original magnetite (*a*) and magnetite with a carbon surface (*b*).

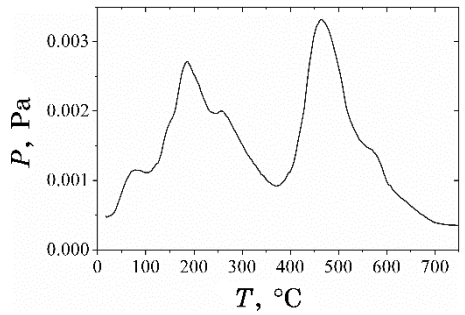

Fig. 2. The p–T curve for pyrolysis of a sample of Fe_3O_4/C obtained by carbonization of a sample of Fe_3O_4/sucrose (magnetite:carbohydrate mass ratio is 1.00/0.45, $t = 200$°C, $p = 506.6$ kPa, $\tau = 6$ h, environment argon).

the surface of NCs because of carbonization were investigated by the TPD MS method. Analysis of mass spectrometric data showed that, under these conditions ($t = 200$°C, $p = 506.6$ kPa, $\tau = 6$ h), complete destruction of the organic modifier does not occur, because the p–T curve has wide diffuse maxima at $t_{max} \cong 180$°C and $t_{max} \cong 470$°C (Fig. 2). These maxima indicate desorption of volatile products formed from dehydration products (mainly anhydrosugars) and other products of thermal conversion of sucrose.

Analysis of mass spectra (Fig. 3, *a*–*c*) and TPD curves (Fig. 3, *d*) obtained in the process of pyrolysis of the Fe_3O_4/C sample showed that, in the temperature range of 150–320°C, heterocyclic compounds of the furan series (furan, methyl furan, furfural, methyl

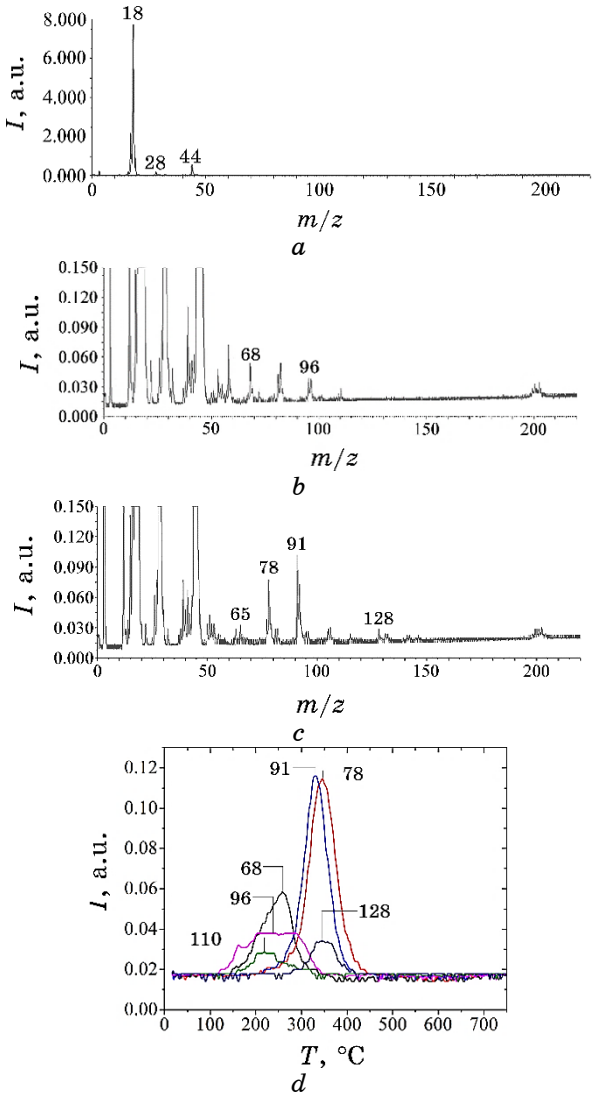

Fig. 3. Pyrolysis of Fe_3O_4/C NCs (carbon source—sucrose). Mass spectra for temperatures: 82°C (*a*), 240°C (*b*), 320°C (*c*); TPD curves (*d*) for molecular ions of furan series compounds: $m/z = 68$ (furan), $m/z = 82$ (methyl furan), $m/z = 96$ (furfural), $m/z = 110$ (methyl furfural), and aromatic compounds: $m/z = 78$ (benzene), $m/z = 91$ (toluene), $m/z = 128$ (naphthalene).

furfural, *etc.* (Fig. 3)) are the main products formed as a result of thermal transformations of the organic coating.

In the temperature range of ≅ 150–320°C, in the mass spectra,

molecular ions of compounds with $m/z = 68$ (furan), $m/z = 82$ (methyl furan), $m/z = 96$ (furfural), $m/z = 110$ (methyl furfural) (Fig. 3, *b*), are observed as the main products of pyrolysis of poly-, oligo- and monosaccharides [43, 44].

The peaks on the TPD curves have a complex shape (Fig. 3, *d*), probably, as a result of the superposition of several peaks, the presence of which may be due to several ways of formation of molecular ions of compounds (Fig. 4). The sucrose molecule consists of monomeric units of glucose and fructose. Accordingly, the activation energies of the formation of furan derivatives from the six-membered glucopyranose cycles will be significantly different from the activation energies of the formation of such derivatives from the five-membered fructose cycles. It is also necessary to take into account anhydro-derivatives of fructose and glucose, the pyrolysis of which produces furan compounds with different activation energies (Fig. 4) and, accordingly, with different temperatures of the maximum desorption rate T_{max}.

Analysis of mass spectra at temperatures in the range of ≅ 270–400°C showed that the second stage of pyrolysis (Fig. 4) was due to the destruction of the modifier with the formation of aromatic compounds. Molecular and fragment ions of the following aromatic compounds were observed in the mass spectra: $m/z = 78$ (benzene), $m/z = 92$ (toluene), $m/z = 91$ (tropylium ion is responsible for the most intense peak in the toluene spectrum), $m/z = 128$ (naphthalene) (Fig. 3, *c*). The peaks of TPD curves at $T_{max} \cong 330$°C ($m/z = 91$),

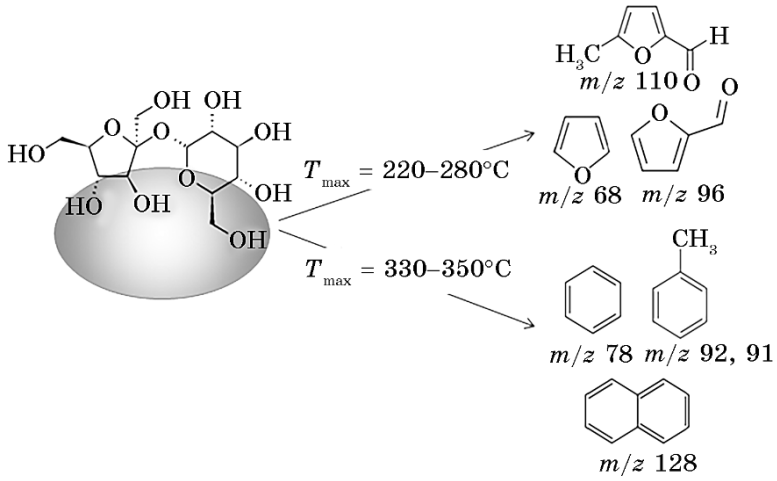

Fig. 4. The main pathways and products of thermal transformations of the modifier of carbohydrate nature (sucrose) on the surface of Fe_3O_4 in the process of the carbon-coating forming.

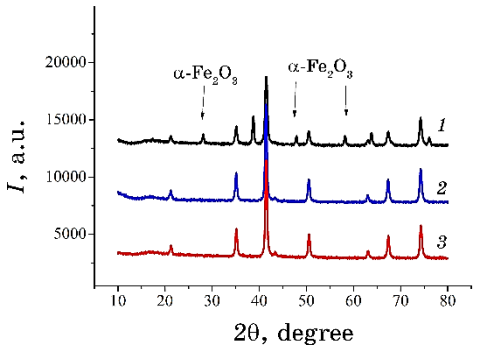

Fig. 5. XRD patterns of Fe_3O_4/Al_2O_3 MNPs' sample: one-time modification (*1*), twice- (*2*) and three-time (*3*) modifications ($t = 500$°C, $\tau = 2$ h, environment argon).

345°C ($m/z = 78$) and 350°C ($m/z = 128$), indicate desorption in the molecular form of aromatic carbohydrates and condensed aromatic carbohydrates.

Thus, XRD and TPD MS studies indicate that pyrolysis at 200°C for 6 h in argon at a pressure of 506.6 kPa is not sufficient for complete carbonization of the organic modifier (sucrose) on the surface of magnetite. Therefore, to protect the magnetite from oxidation under the influence of the elevated temperature required to obtain a high-quality carbon shell, an additional modification of the surface of the magnetite with aluminium isopropylate was performed.

The amount of alumina sufficient to protect the magnetite when heated to 500°C for 2 h in an argon atmosphere was optimized by XRD control of phase content studies of the samples (Fig. 5).

Thus, it was shown that one-time modification does not prevent partial oxidation and formation of the α-Fe_2O_3 phase during heat treatment of the samples (ICDD No. 73-603) (Fig. 5, *a*). The use of twice- and three-modifications allows to obtain coatings that protect the magnetite from oxidation due to heat treatment, as evidenced by the presence on the diffraction patterns of reflexes related only to the Fe_3O_4 phase (JCPDS No. 88-315) (Fig. 5, *b*, *c*).

Furthermore, the diffractogram of the $Fe_3O_4/Al_2O_3/C$ NC sample, obtained with 2 layers of aluminium oxide and pyrolysis with sucrose, differs from the diffractogram of Fe_3O_4/Al_2O_3 MPCs, obtained with only double Al_2O_3 modification, by the lower intensity of the diffraction Fe_3O_4 peaks. This indicates the formation of an amorphous carbon-containing coating on the surface of $Fe_3O_4/Al_2O_3/C$ NC sample (Fig. 6).

That is, the two-layer coating of alumina is sufficient to protect

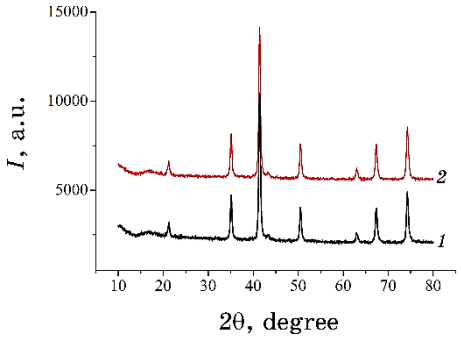

Fig. 6. XRD patterns of Fe_3O_4/Al_2O_3 MNPs' sample (*1*), obtained by twice time modification, and $Fe_3O_4/Al_2O_3/C$ NCs (*2*) (t = 500°C, τ = 2 h, environment argon).

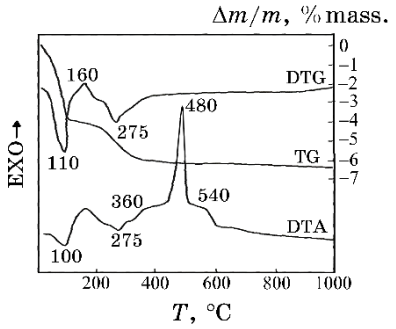

Fig. 7. TGA measurement for Fe_3O_4 MNPs' samples.

the magnetite from oxidation during the pyrolysis of Fe_3O_4/Al_2O_3/sucrose composites. All further studies were performed on Fe_3O_4/Al_2O_3 samples obtained by double modification.

The increase in the transition temperature of magnetite to hematite was also confirmed by the DTA method.

This is derivatogram of the original nanodispersed magnetite presented in Fig. 7 and registered in air. When on DTA curve, there are having place next temperature effects—one was characterized by an endothermic effect at a temperature of 1000°C being accomplished by weight-loss effect (on TG one), and those are owns corresponding minimum on DTG one too. This thermal effect refers to the loss of physically bonded water.

Next, clear endothermic minimum appears at temperature of 275°C, in the range of 200–380°C (DTA curve), and there is one corresponding minimum on the DTG one, which linked with the removal of water, and, as a result, to the condensation of hydroxyl groups on the particle surface. There are available also exothermic

maxima: first, weak at 360°C, and second, intense at 480°C, may be attributed to thermal phase transitions of magnetite.

There are available such of exothermic maxima—first, weak at a temperature of 340°C, may be referred to magnetite–to–maghemite (γ-Fe_2O_3) phase oxidation process, which being particularly created during heating in derivatograph oven and derivatogram registration, and second, intense at a temperature of 480°C, may be corresponding to magnetite–to–hematite transition (α-Fe_2O_3) one, which may be attributed to thermal phase transformations of magnetite. Derivatograms of thermal transformations of the Fe_3O_4/Al_2O_3 NCs are shown in Fig. 8.

There are curves of the complete thermal analysis, which is reflecting the transformation of both composite components: for both, magnetite (core) as well as shell, where aluminium isopropylate polycondensation process is, when, at involving of functional groups, one goes on during heating. There are minima on DTA and DTG curves (Fig. 8, *a*) at a temperature of 110°C, which are corresponding to the volatile products removal such as water and isopropyl alcohol. Narrow low-intensity minimum at 210°C on the ascending branch of main one and at 110°C on the DTG curve can probably be attributed to the residual aluminium isopropylate removal. There is a minimum on the DTG curve at a temperature of 300°C; this can be associated with the condensation of hydroxyl groups on the magnetite surface, and water removal. Next, extensive minimum on DTG may be responsible to the condensation of –Al–OH groups, when with following formation process of –Al–O–Al– groupings. There are two exothermic peaks at 210 and 310°C; they can be associated with redox processes of both components: magnetite–to–maghemite oxidation and thermal destruction of isopropyl radicals.

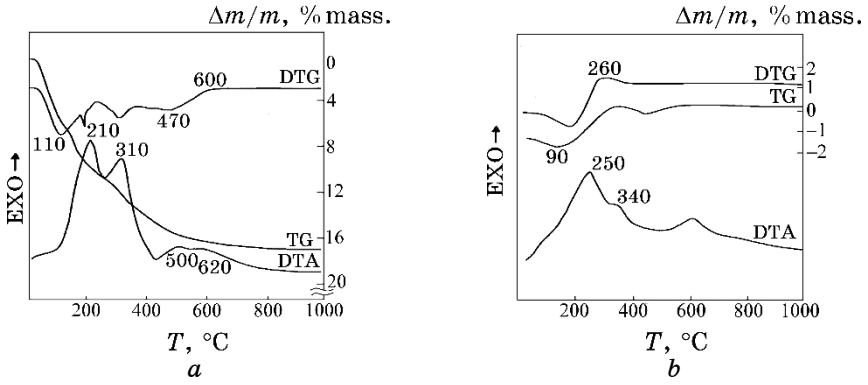

Fig. 8. TGA measurement of NCs' samples: Fe_3O_4/Al_2O_3 (*a*), Fe_3O_4/Al_2O_3 (*b*), annealed at 500°C for 2 h.

There are exothermic peaks in the temperature range 500–620°C, and those are regarding to the magnetite–to–hematite transition process. An exothermic peak at 660°C is observed also for the sample, which firstly dried and, then, annealed at 500°C in a stream of argon (Fig. 8, *b*).

Temperature of the exothermic peak increases, when characterizing magnetite–to–hematite oxidation process; there was also observed such a phenomenon in Ref. [45], where magnetite was modified with layers of silicon and titanium oxides. Such a shift may be indicating on the formation of a protective oxide shell on magnetite NPs.

When regarding for the sample annealed at 500°C in a stream of argon (Fig. 8, *b*), in the temperature range of 100–300°C, there is a slight mass increasing, which can be caused by oxygen connection, *i.e.*, oxidation process. There is pyrolysis of the organic part of the modifier exists, namely, for isopropyl radicals, which can create a reducing atmosphere for iron oxides. When at heating in air during thermogram registration, the oxidation process reflects on the DTA curve in form of exothermic maximum, and as mass increase on the TG one, as well as the corresponding maximum on the DTG one. It is likely that a small part on the surface layer of magnetite particles being subjected to redox effects.

The completeness of the carbonization of the surface layer of the carbohydrate was evaluated using the method of TPD MS. Significant reduction of peak intensity on p–T curves on TPD curves (Fig. 9) and analysis of mass spectra (detected CO_2, CO and H_2O, no characteristic of thermal destruction of carbohydrates furan derivatives and other products) (Fig. 10) for samples subjected to pyrolysis at 500°C in an argon stream, compared with samples whose pyrolysis

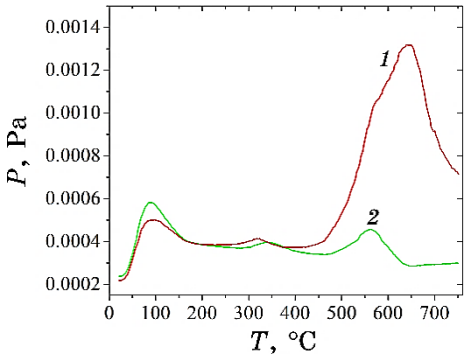

Fig. 9. The p–T curves for pyrolysis of a sample of $Fe_3O_4/Al_2O_3/C$ (*1*) obtained by carbonization of a sample of Fe_3O_4/Al_2O_3/sucrose (magnetite:carbohydrate mass ratio is 1.00/0.45) and Fe_3O_4/Al_2O_3 (*2*) (t = 500°C, τ = 2 h, environment argon).

was carried out by lower temperature (Fig. 2), indicates the effective carbonization of the carbohydrate modifier.

According to the results of image processing of ensembles of Fe_3O_4 NPs, Fe_3O_4/Al_2O_3 and $Fe_3O_4/Al_2O_3/C$ NCs, obtained by the TEM method, the similarity of shape and their average size were established: for Fe_3O_4, 10.5 nm; for Fe_3O_4/Al_2O_3 NCs, 14.5 nm; for $Fe_3O_4/Al_2O_3/C$ NCs, 15.5 nm (Fig. 11).

Using the principles of magnetic granulometry and the superparamagnetic properties of Fe_3O_4 as a probe [24–26, 29, 32], the magnetic and dimensional parameters of Fe_3O_4/Al_2O_3 and $Fe_3O_4/Al_2O_3/C$ nanostructures were studied. Using these approaches and data of magnetic measurements on the value of $\sigma_s^{NC}/\sigma_s^{Fe_3O_4}$, the diameters and thickness of the shells of the synthesized nanostructures were calculated.

Magnetic hysteresis loops measured at room temperature (≈ 26°C) for the NPs and composites are presented in Fig. 12.

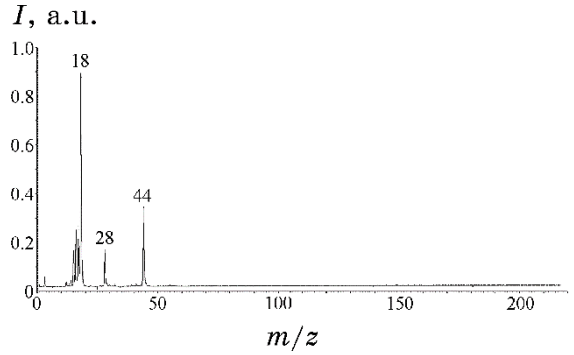

Fig. 10. Mass spectra of $Fe_3O_4/Al_2O_3/C$ NCs for temperature of 235°C (magnetite:carbohydrate mass ratio is 1.00/0.45, pyrolysis $t = 500$°C, $\tau = 2$ h, environment argon).

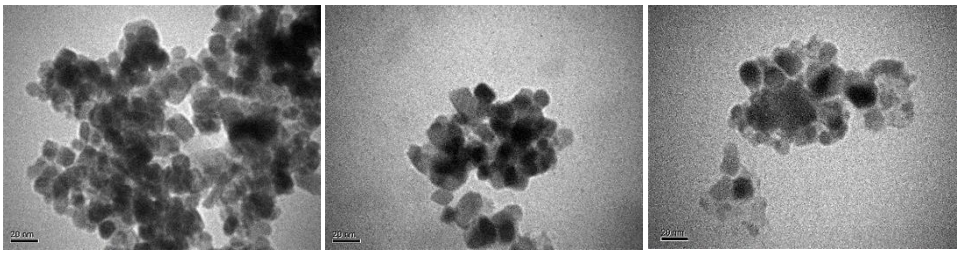

Fig. 11. TEM images: Fe_3O_4 (*a*); Fe_3O_4/Al_2O_3 (*b*); $Fe_3O_4/Al_2O_3/C$ (*c*). Scale bar of 20 nm.

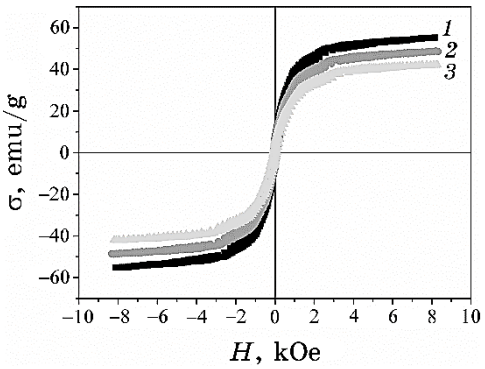

Fig. 12. Magnetic hysteresis loops for the samples: Fe_3O_4 (*1*); Fe_3O_4/Al_2O_3 (*2*) and Fe_3O_4/Al_2O_3/C NCs (*3*).

TABLE 1. Magnetic characteristics of Fe_3O_4, Fe_3O_4/Al_2O_3, Fe_3O_4/Al_2O_3/C NCs.

Samples	$\sigma_{(H=8\ kOe)}$, emu·g^{-1}	σ_r, emu·g^{-1}	σ_s, emu·g^{-1}	σ_r/σ_s	$\sigma_s^{NC}/\sigma_s^{Fe_3O_4}$	H_c, Oe
Fe_3O_4	55.6*	7.37*)	57.9	0.12	1	81
Fe_3O_4/Al_2O_3	48.7*	6.31*)	51.0	0.12	0.88	82
Fe_3O_4/Al_2O_3/C	42.4*	5.36*)	44.3	0.12	0.76	94

Note: *) error ±2.5%; H_c [Oe] is coercive force; σ_s [emu·g^{-1}] is specific saturation magnetization (its value is obtained by extrapolation of the experimental curve $\sigma(H^{-1})$ to the *y*-axis); $\sigma_{(H\ 8\ kOe)}$ [emu·g^{-1}] is specific magnetization in the field of 8 kOe; σ_r [emu·g^{-1}] is residual specific magnetization; σ_r/σ_s is relative residual magnetization; $\sigma_s^{NC}/\sigma_s^{Fe_3O_4}$ is mass fraction of magnetite in NC.

In Table 1, the magnetic characteristics of Fe_3O_4, Fe_3O_4/Al_2O_3 and Fe_3O_4/Al_2O_3/C NCs are presented.

The value $\sigma_s = 57.9$ emu·g^{-1} (Table 1) for Fe_3O_4 samples is characteristic of nanodispersed magnetite [26, 27], and a decrease in this value for the Fe_3O_4/Al_2O_3 (51.0 emu·g^{-1}) and Fe_3O_4/Al_2O_3/C/C (42.4 emu·g^{-1}) structures are consistent with the corresponding changes in the mass fraction of $\sigma_s^{NC}/\sigma_s^{Fe_3O_4}$ magnetite in the NCs and indicates the presence of a nonmagnetic shell around the magnetic core.

It is seen that the dimensions of the studied nanostructures, determined by the methods of statistical processing of TEM images (Fig. 11), are consistent with the corresponding values obtained by magnetic measurements (Table 2).

Studies have shown that the magnetic characteristics of single-domain magnetite are virtually unchanged, and the properties of Fe_3O_4/Al_2O_3/C NCs correspond to the sequential formation of Al_2O_3 and C shells because of modifications.

TABLE 2. The average diameters (d^-_{TEM}, d^-_M) and the thickness of the shells of nanostructures h^-_M determined by electron microscopic (*TEM*) and magnetic (*M*) measurements.

Samples	d^-_{TEM}, nm	d^-_M, nm	h^-_M, nm
Fe_3O_4	10.5	10.5	0
Fe_3O_4/Al_2O_3	14.5	10.5	$2(Al_2O_3)$
$Fe_3O_4/Al_2O_3/C$	15.5	10.5	$2.5(2Al_2O_3 + 0.5C)$

TABLE 3. The value of the specific surface area and pore size of the magnetite-based nanostructures.

Samples	Langmuir surface area, $m^2 \cdot g^{-1}$	Total pore volume, $mm^3 \cdot g^{-1}$	Micropore volume, $mm^3 \cdot g^{-1}$	Micropore area, $m^2 \cdot g^{-1}$	Non-microporous surface area, $m^2 \cdot g^{-1}$
Fe_3O_4	110	313.24	1.16	3.298	82.93
Fe_3O_4/Al_2O_3 (annealed)	104	277.10	0.91	2.58	76.70
$Fe_3O_4/Al_2O_3/C$	160	248.52	19.27	54.70	60.07

Using the obtained average values of the size of the original magnetite, Fe_3O_4/Al_2O_3 and $Fe_3O_4/Al_2O_3/C$ NCs and their shells, using the results of TEM studies and magnetic measurements, it was calculated the density of the Al_2O_3 shell, *i.e.*, 3.23 g/cm^3, which is in good agreement for the γ-Al_2O_3 phase [46, 47].

The values of the specific surface area and pore size of the studied nanostructures, which were determined by the method of thermal desorption of nitrogen, are shown in Table 3. For the Fe_3O_4/Al_2O_3 and $Fe_3O_4/Al_2O_3/C$ samples, annealing of the coating and pyrolysis of the carbohydrate were carried out under the same conditions: $T = 500°C$, $\tau = 2$ h, environment argon.

Table 3 shows that annealing Fe_3O_4/Al_2O_3 NCs reduces, compared to unmodified magnetite, the specific surface area to 104 $m^2 \cdot g^{-1}$ with a micropore volume of 0.91 $mm^3 \cdot g^{-1}$ and a micropore area of 2.58 $m^2 \cdot g^{-1}$. This can be explained by the formation around the magnetite core of a polymer structure of alumina, the thermal annealing of which leads to better ordering of the Al_2O_3 layer, its compaction and release of isopropylate residues, which, in turn,

given the coating thickness (2 nm, Table 2) and leads to a decrease in the surface of the NCs.

The process of carbonization of the layer carbohydrate increases the specific surface of NCs to 160 $m^2 \cdot g^{-1}$ with a micropore volume of 19.27 $mm^3 \cdot g^{-1}$ and a micropore surface area of 54.70 $m^2 \cdot g^{-1}$. Given the value of the average thickness of the carbon layer (0.5 nm, Table 2) on the surface of Fe_3O_4/Al_2O_3 NCs and the significant contribution of carbon micropores (54.70 $m^2 \cdot g^{-1}$) in the specific surface of $Fe_3O_4/Al_2O_3/C$ NCs (160 $m^2 \cdot g^{-1}$), we can conclude about the heterogeneous structure of the carbon coating.

Testing of the adsorption activity of $Fe_3O_4/Al_2O_3/C$ NCs was performed using methylene blue (MB). Experimental results of kinetic studies were used to determine the limiting stage and the possible mechanism of adsorption. Correspondence to the kinetic model was established by the method of linearization in the coordinates of integral equations and statistical methods with the determination of the correlation coefficient [48–50]. To model the adsorption kinetics, the Weber–Morris and Boyd's diffusion models, Lagergren pseudo-first-order models, Ho and McKay's pseudo-second-order models, and Yelovich's model were used.

Analysis of the experimental kinetic dependence (Fig. 13, *a*) indicates a mixed-diffusion mechanism of kinetics. The model of the pseudo-second order with a high correlation coefficient $r^2 = 0.993$ (Fig. 13, *b*) and similar to the experimental value of A_{calc} (Table 4) agrees with the parameters of adsorption of molecules and ionic forms of MB.

Experimental results of the study of the adsorption activity of $Fe_3O_4/Al_2O_3/C$ NCs relative to MB in the concentration range $C_0 = 0.028–0.148$ $mg \cdot ml^{-1}$ were used to construct the isotherm (Fig. 14) and analysed for compliance with the adsorption model.

The value of the correlation coefficient (r^2), the close values of the experimental and calculated values of A indicate the correctness of the use of the Freundlich model to describe the adsorption processes (Table 5).

The calculated isotherm parameters and kinetic characteristics of adsorption indicate the process on non-equivalent energy centres of the surface by the mixed-diffusion mechanism.

The results of the work may be relevant for use in the development of new magnetically controlled adsorption materials for technical, technological, environmental and medical–biological purposes, medical test-systems, theranostic systems of targeted delivery, *etc.*

4. CONCLUSIONS

The processes of pyrolytic carbonization of sucrose-containing coat-

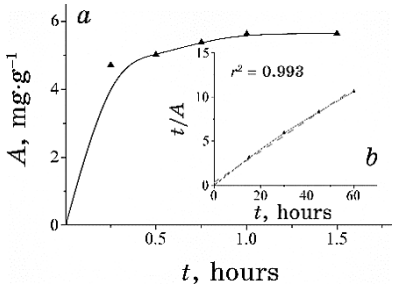

Fig. 13. Experimental kinetic curve of MB adsorption on the surface of $Fe_3O_4/Al_2O_3/C$ NCs (*a*) and linearized form in the co-ordinates of the pseudo-second order model (*b*).

TABLE 4. Kinetic parameters of MB adsorption on the surface of $Fe_3O_4/Al_2O_3/C$ NCs.

Kinetic model of the pseudo-second order equation $t/A = 1/kA^2_{eq} + t/A_{eq}$ Linear form $t/A–t$							
C_0, mg·ml^{-1}	C_{eq}, mg·ml^{-1}	A_{exp}, mg·g^{-1}	A_{calc}, mg·g^{-1}	R, %	k, g·(mg·min)$^{-1}$	V_0, mg·(g·min)$^{-1}$	r^2
0.034	$3.1 \cdot 10^{-6}$	5.67	5.75	99.9	0.077	2.476	0.99

Note: A_{exp} is experimental adsorption capacity [mg·g^{-1}]; A_{calc} is calculated adsorption capacity [mg·g^{-1}]; k is pseudo-second order adsorption equilibrium rate constant [g·(mg·min)$^{-1}$]; V_0 is initial adsorption rate [mg·(g·min)$^{-1}$].

ings on the surface of single-domain magnetite and Fe_3O_4/Al_2O_3 NCs have been studied. In the mass spectra of volatile pyrolysis products of coatings heat-treated at 500°C for 2 h in an argon stream, the main pyrolysis products are CO_2, CO and water that indicates the efficiency of the carbonization process of the carbohydrate coating. It is revealed that the used heat-treatment mode does not lead to deterioration of the magnetic characteristics of magnetite under the condition of preliminary creation on its surface of a protective layer of alumina. As shown, the carbonization of sucrose-containing coatings on the surface of Fe_3O_4/Al_2O_3 NCs under these conditions is complete, and the final product of the process is $Fe_3O_4/Al_2O_3/C$ NCs.

The TEM method showed that, in all studied samples of Fe_3O_4,

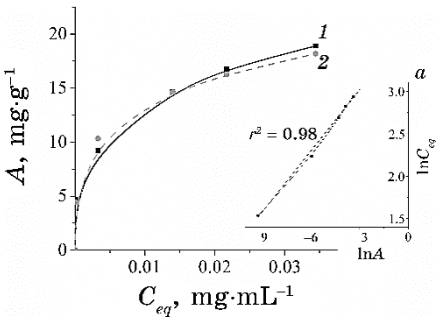

Fig. 14. Isotherms of MB adsorption on $Fe_3O_4/Al_2O_3/C$ NCs: obtained from adsorption experiment (*1*); calculated from the parameters of the Freundlich equation (*2*); linearized form of Freundlich isotherm (*a*).

TABLE 5. Parameters of MB adsorption on $Fe_3O_4/Al_2O_3/C$ NCs calculated using Freundlich models.

Equation	$A_p = K_F C_p^{1/n}$				
Linearized form	$\ln A_p = \ln K_F + (1/n)\ln C_p$				
Calculated parameters	A_{exp}, mg·g^{-1}	A_{calc}, mg·g^{-1}	K_F	$1/n$	r^2
$C_0 = 0.028–0.148$ mg·ml^{-1}	18.9	18.17	40.89	0.24	0.98

Fe_3O_4/Al_2O_3, $Fe_3O_4/Al_2O_3/C$, the shape of the NPs is similar; their average sizes are consistent with the data of magnetic measurements. The values of the specific saturation magnetization σ_s of Fe_3O_4/Al_2O_3 (48.7 emu·g^{-1}) and $Fe_3O_4/Al_2O_3/C$ (42.4 emu·g^{-1}) NCs are consistent with the corresponding changes in the mass fraction $\sigma_s^{NC}/\sigma_s^{Fe_3O_4}$ of magnetite in these structures. Data from TEM studies and magnetic measurements indicate the formation of the structure of Fe_3O_4/Al_2O_3 and $Fe_3O_4/Al_2O_3/C$ NCs by the core–shell type. Testing of the adsorption activity of the carbon surface of $Fe_3O_4/Al_2O_3/C$ NCs was performed using MB. The results of the work may be relevant for use in the development of new magnetically controlled adsorption materials for technical, technological, environmental and medical–biological purposes, medical test-systems, theranostic systems of targeted delivery, *etc.*

REFERENCES

1. S. V. Mishchenko and A. G. Tkachev, *Uglerodnyye Nanomaterialy. Proizvodstvo, Svoystva, Primenenie* [Carbon Nanomaterials. Production, Properties, Application] (Moskva: Mashinostroyenie: 2008), p. 320 (in Russian).
2. Yu. I. Sementsov, *Formuvannya Struktury ta Vlastyvostey sp²-Vuhletsevykh*

Nanomaterialiv ta Funktsional'nykh Kompozytiv za Yikh Uchastyu [Formation of Structure and Properties of sp^2-Carbon Nanomaterials and Functional Composites with Their Participation] (Kyiv: Interservice: 2019), p. 364 (in Ukrainian).

3. O. M. Sedov, V. V. Holod, S. M. Makhno, O. M. Lisova, M. V. Abramov, S. P. Turanska et al., *Metallofiz. Noveishie Tekhnol.*, **41**: 1153 (2019) (in Ukrainian); https://doi.org/10.15407/mfint.41.09.1153
4. P. Mierczynski, S. V. Dubkov, S. V. Bulyarskii, A. A. Pavlov, S. N. Skorik, A. Y. Trifonov et al., *J. Mater. Sci. Technol.*, **34**, No. 3: 472 (2018); https://doi.org/10.1016/j.jmst.2017.01.030
5. S. Dubkov, I. Gavrilin, A. Dronov, A. Trifonov, A. Dudin, A. Sirotina et al., *Materials Today–Proc.*, **5**: 15943 (2018); https://doi.org/10.1016/j.matpr.2018.06.061
6. O. M. Lisova, M. V. Abramov, S. M. Makhno, and P. P. Gorbyk, *Metallofiz. Noveishie Tekhnol.*, **40**: 625 (2018); https://doi.org/10.15407/mfint.40.05.0625
7. P. V. Ratnikov and A. P. Silin, *Physics-Uspekhi*, **61**, No. 12: 1139 (2018); https://doi.org/10.3367/UFNr.2017.11.0382318
8. P. M. Sokolov, M. A. Zvaigzne, V. A. Krivenkov, A. P. Litvin, A. V. Baranov, A. V. Fedorov et al., *Russ. Chem. Rev.*, **88**: 370 (2019); http://dx.doi.org/10.1070/RCR4859
9. M. A. Perederiy, Yu. A. Noskova, M. S. Karaseva, and P. N. Konovalov, *Solid Fuel Chem.*, **6**: 36 (2009); https://doi.org/10.3103/S0361521909060056
10. V. G. Nikolayev, S. V. Mikhalovsky, and N. M. Gurina, *Efferent Therapy*, **11**: 3 (2005) (in Russian).
11. K. Yang, L. Zhu, and B. Xing, *Environ. Sci. Technol.*, **40**: 1855 (2006); https://doi.org/10.1021/es052208w
12. *Application of Enterosorption in Complex Therapy of Liver Diseases* (accessed 8 November 2020); https://www.apteka.ua/article/14310
13. V. N. Mishchenko, M. T. Kartel, V. A. Lutsenko, A. D. Nikolaichuk, N. V. Kusyak, O. M. Korduban et al., *Surface*, **2**: 276 (2010) (in Ukrainian); http://dspace.nbuv.gov.ua/handle/123456789/39341
14. A.-H. Lu, W.-C. Li, N. Matoussevitch, B. Spliethoff, H. Bönnemann, and F. Schüth, *Chem. Commun.*, **1**: 98 (2005); https://doi.org/10.1039/B414146F
15. E. Kim, K. Lee, Y.-M. Huh, and S. Haam, *J. Mater. Chem. B*, **1**: 729 (2013); https://doi.org/10.1039/C2TB00294A
16. P. P. Gorbyk, N. V. Kusyak, A. L. Petranovskaya, E. I. Oranskaya, N. V. Abramov, and N. M. Opanashchuk, *Him. Fiz. Tehnol. Poverhni*, **9**: 176 (2018); https://doi.org/10.15407/hftp09.02.176
17. Y. Xu, W. E. Heberlein, M. Mahmood, A. I. Orza, A. Karmakar, Th. Mustafa et al., *J. Mater. Chem.*, **22**: 20128 (2012); https://doi.org/10.1039/C2JM32792A
18. M. Zhu, C. Wang, D. Menga, and G. Diao, *J. Mater. Chem. A*, **1**: 2018 (2013); https://doi.org/10.1039/C2TA00669C
19. L. Wan, D. Yan, X. Xu, J. Li, T. Lu, Y. Gao et al., *J. Mater. Chem. A*, **6**: 24940 (2018); https://doi.org/10.1039/C8TA06482B
20. P. P. Gorbyk, *Nanosistemi, Nanomateriali, Nanotehnologii*, **11**, Iss. 2: 323 (2013).

21. P. P. Gorbyk, I. V. Dubrovin, A. L. Petranovska, M. V. Abramov, D. G. Usov, and L. P. Storozhuk, *Chemical Construction of Polyfunctional Nanocomposites and Nanorobots for Medico-Biological Applications, Nanomaterials and Supramolecular Structures. Physics, Chemistry, and Applications* (Eds. A. P. Shpak and P. P. Gorbyk) (Netherlands: Springer: 2009), pp. 63–78; https://doi.org/10.1007/978-90-481-2309-4_6
22. P. P. Gorbyk, L. B. Lerman, A. L. Petranovska, and S. P. Turanska, *Magnetosensitive Nanocomposites with Functions of Medicobiological Nanorobots: Synthesis and Properties, Advances in Semiconductor Research: Physics of Nanosystems, Spintronics and Technological Applications.* (Eds. D. P. Adorno and S. Pokutnyi) (New York: Nova Science Publishers: 2014), pp. 161–198.
23. P. P. Gorbyk, L. B. Lerman, A. L. Petranovska, S. P. Turanska, Ie. V. Pylypchuk, *Magnetosensitive Nanocomposites with Hierarchical Nanoarchitecture as Biomedical Nanorobots: Synthesis, Properties, and Application, Fabrication and Self-Assembly of Nanobiomaterials, Applications of Nanobiomaterials* (Ed. A. Grumezescu) (Amsterdam: Elsevier: 2016), pp. 289–334.
24. M. V. Abramov, A. P. Kusyak, O. M. Kaminskiy, S. P. Turanska, A. L. Petranovska, N. V. Kusyak et al., *Horiz. in World Phys.*, **293**: 1 (2017).
25. M. V. Abramov, S. P. Turanska, and P. P. Gorbyk, *Metallofiz. Noveishie Tekhnol.*, **40**: 423 (2018); https://doi.org/10.15407/mfint.40.04.0423
26. M. V. Abramov, S. P. Turanska, and P. P. Gorbyk, *Metallofiz. Noveishie Tekhnol.*, **40**: 1283 (2018); https://doi.org/10.15407/mfint.40.10.1283
27. A. L. Petranovska, N. V. Abramov, S. P. Turanska, P. P. Gorbyk, A. N. Kaminskiy, and N. V. Kusyak, *J. Nanostruct. Chem.*, **5**: 275 (2015); https://doi.org/10.1007/s40097-015-0159-9
28. M. V. Abramov, A. L. Petranovska, N. V. Kusyak, A. P. Kusyak, N. M. Opanashchuk, S. P. Turanska et al., *Funct. Mater.*, **27**, No. 2: 283 (2020); https://doi.org/10.15407/fm27.02.283
29. N. V. Abramov, S. P. Turanska, A. P. Kusyak, A. L. Petranovska, and P. P. Gorbyk, *J. Nanostruct. Chem.*, **6**: 223 (2016); https://doi.org/10.1007/s40097-016-0196-z
30. P. P. Gorbyk, *Him. Fiz. Tehnol. Poverhni*, **11**, No. 1: 128 (2020); https://doi.org/10.15407/hftp11.01.128
31. R. Zhang and H. Olin, *Mater. Sci. Eng. C*, **32**: 1247 (2012); https://doi.org/10.1016/j.msec.2012.03.016
32. M. V. Abramov, S. P. Turans'ka, and P. P. Gorbyk, *Nanosistemi, Nanomateriali, Nanotehnologii*, **18**, Iss. 3: 505 (2020) (in Ukrainian); https://doi.org/10.15407/nnn.18.03.505
33. T. Sakaki, M. Shibata, T. Miki, H. Hirosue, and N. Hayashi, *Bioresource Technol.*, **58**: 197 (1996); https://doi.org/10.1016/S0960-8524(96)00099-5
34. G.-Y. Mao, W.-J. Yang, F.-X. Bu, D.-M. Jiang, Z.-J. Zhao, Q.-H. Zhang et al., *J. Mater. Chem. B*, **2**: 4481 (2014); https://doi.org/10.1039/C4TB00394B
35. L. Qu, T. Han, Z. Luo, C. Liu, Y. Mei, and T. Zhu, *J. Phys. Chem. Solids*, **78**: 20 (2015); https://doi.org/10.1016/j.jpcs.2014.10.019
36. T. Sakaki, M. Shibata, T. Miki, H. Hirosue, and N. Hayashi, *Bioresource*

Technol., **58**, No. 2: 197 (1996); https://doi.org/10.1016/S0960-8524(96)00099-5
37. S. Liang, K. Chen, J. Han, and B. Wu, *Mater. Sci. Eng.*, **562**: 12022 (2019); https://doi.org/10.1088/1757-899X/562/1/012022
38. P. Wang, M. Gao, H. Pan, J. Zhang, C. Liang, J. Wang et al., *J. Power Sources.*, **239**: 466 (2013); https://doi.org/10.1016/j.jpowsour.2013.03.073
39. P. Selwood, *Magnetochemistry Access mode: by Subscription* (accessed 08 November 2020); https://biblioclub.ru/index.php?page=book&id=213957
40. A. L. Petranovska, D. G. Usov, M. V. Abramov, Yu. O. Demchenko, and O. M. Corduban, *Him. Fiz. Tehnol. Poverhni*, **13**: 310 (2007); http://dspace.nbuv.gov.ua/handle/123456789/146644
41. T. Kulik, B. Palianytsia, and M. Larsson, *Catalysts*, **10**, No. 2: 1 (2020); https://doi.org/10.3390/catal10020179
42. K. Kulyk, B. Palianytsia, J. D. Alexander, L. Azizova, M. Borysenko, M. Kartel et al., *Chem. Phys. Chem.*, **18**, No. 14: 1943 (2017); https://doi.org/10.1002/cphc.201601370
43. S. Nanda, P. Mohanty, J. A. Kozinski, and A. K. Dalai, *Energy Environ. Res.*, **4**, No. 3: 21 (2014); https://doi.org/10.5539/eer.v4n3p21
44. T. Kulyk, *Polym. J.*, **40**: 166 (2018) (in Ukrainian); https://doi.org/10.15407/polymerj.40.03.166
45. L. S. Semko, P. P. Gorbyk, L. P. Storozhuk, A. M. Korduban, and L. S. Dzyubenko, *Him. Fiz. Tehnol. Poverhni*, **13**: 370 (2007).
46. A. M. Abyzov, *New Refractories*, **1**: 16 (2019); http://dx.doi.org/10.17073/1683-4518-2019-1-16-23
47. *Alumina and Its Modifications* (accessed 11 November 2020); https://liv-unikon.com.ua/ru/glynozem-y-ego-modyfykatsyy.html
48. J. P. Simonin and J. Boute, *Rev. Mex. Ing. Quim.*, **15**, No. 1: 161 (2016).
49. Y. S. Ho, J. C. Y. Ng, and G. McKay, *Separ. Purif. Method*, **29**, No. 2: 189 (2000); https://doi.org/10.1081/SPM-100100009
50. S. Douven, C. A. Paez, and C. J. Gommes, *J. Colloid. Interface Sci.*, **448**: 437 (2015); https://doi.org/10.1016/j.jcis.2015.02.053